

1 **Prediction of transporter-mediated drug-drug interactions**
2 **and phenotyping of hepatobiliary transporters involved in**
3 **the clearance of E7766, a novel macrocycle-bridged**
4 **dinucleotide**

5 Rongrong Jiang^{*}, Andrew Hart¹, Laurette Burgess, Dae-Shik Kim, Weidong Lai², Vaishali Dixit^{*}

6 *Drug Metabolism and Pharmacokinetics, Eisai Inc, Massachusetts, USA (R.J., V.D., G.L., A.H.)*

7 *Genetics Guided Dementia Discovery, Eisai Inc, Massachusetts, USA (L.B., D.S.K.)*

8 ¹*Current Address: Wave Life Sciences, Massachusetts, USA*

9 ²*Current Address: Triplet Therapeutics, Massachusetts, USA*

10 ^{*}*Co-corresponding authors*

11 **Running Title:** Transporter-mediated drug-drug interactions for E7766

12 **Co-corresponding authors**

13 Dr. Rongrong Jiang, Drug Metabolism and Pharmacokinetics, Eisai Inc, Cambridge

14 Massachusetts, USA. Tel: (857) 829-6063; E-mail: Rongrong_jiang@eisai.com

15 Dr. Vaishali Dixit, E-mail: dixitv77@gmail.com

16

17

18 Number of text pages: 25

19 Words in the Abstract: 243

20 Words in the Introduction: 591

21 Words in the Discussion: 1341

22 Number of references: 35

23 Number of Tables: 5

24 Number of Figures: 5

25 Number of Supplemental Tables: 4

26 Number of Supplemental Figures: 3

27

28 **List of abbreviations**

29 $A_{e\text{ fecal}}$, amount excreted in feces; $A_{e\text{ biliary}}$, amount excreted in bile; $A_{e\text{ renal}}$, amount excreted in
30 urine; BCRP, breast cancer resistance protein; BSEP, bile salt export pump; CL_{biliary} ,
31 hepatobiliary excretory clearance; CL_{fecal} , fecal excretory clearance; CL_{int} , intrinsic clearance;
32 $CL_{\text{tot,p}}$, total plasma clearance; CL_{renal} , renal excretory clearance; K_m , Michaelis-Menten constant;
33 MDR, multidrug resistance; MRP, multidrug resistance-associated protein; NCEs, new chemical
34 entities; NTCP, Na^+ /taurocholate cotransporting polypeptide; OAT, organic anion transporter;
35 OATP, organic anion transporting polypeptide; OCT, organic cation transporter; PBPK,
36 physiologically based pharmacokinetic; PK, pharmacokinetic; V_{max} , maximum transport velocity;
37 V_{SS} , distribution volume at steady state.

38

39 **Abstract**

40 E7766 represents a novel class of macrocycle-bridged dinucleotides, and is under clinical
41 development for immuno-oncology. In this report, we identified mechanism of systemic
42 clearance E7766, investigated the hepatobiliary transporters involved in the disposition of E7766
43 and potential drug interactions of E7766 as a victim of organic anion transporting polypeptide
44 (OATP) inhibitors. In bile-duct cannulated (BDC) rats and dogs, E7766 was mainly excreted
45 unchanged in bile (>80%) and to a lesser extent in urine (<20%). Sandwich cultured human
46 hepatocytes (SCHH), transfected cells and vesicles were used to phenotype the hepatobiliary
47 transporters involved in the clearance of E7766. SCHH data showed temperature-dependent
48 uptake of E7766, followed by active biliary secretion. In vitro transport assays using transfected
49 cells and membrane vesicles confirmed that E7766 was a substrate of OATP1B1, OATP1B3 and
50 multidrug resistance-associated protein 2 (MRP2). Phenotyping studies suggested predominant
51 contribution of OATP1B3 over OATP1B1 in the hepatic uptake of E7766. Studies in
52 OATP1B1/1B3 humanized mice showed that plasma exposure of E7766 increased 4.5-fold when
53 coadministered with Rifampicin. Physiologically based pharmacokinetic (PBPK) models built
54 upon two independent bottom-up approaches predicted elevation of E7766 plasma exposure
55 when administered with Rifampicin, a clinical OATP inhibitor. In conclusion, we demonstrate
56 that OATP-mediated hepatic uptake is the major contributor to the clearance of E7766 and
57 inhibition of OATP1B may increase its systemic exposure. Predominant contribution of
58 OATP1B3 in the hepatic uptake of E7766 was observed, suggesting polymorphisms in
59 OATP1B1 would be unlikely to cause variability in the exposure of E7766.

60

61 **Significance Statement**

62 Understanding the clearance mechanisms of new chemical entities is critical to predicting human
63 pharmacokinetics and drug interactions. A physiologically based pharmacokinetic model that
64 incorporated parameters from mechanistic in vitro and in vivo experiments was used to predict
65 pharmacokinetics and drug interactions of E7766, a novel dinucleotide drug. The findings
66 highlighted here may shed a light on the pharmacokinetic profile and transporter-mediated drug
67 interaction propensity of other dinucleotide drugs.

68

69 **Introduction**

70 Stimulator of interferon genes (STING) is an important innate immune sensor, and activation of
71 STING plays a critical role in controlling cancer development by bridging the innate and
72 adaptive immunities (Corrales et al., 2016; Woo et al., 2014). Significant efforts have been made
73 by several pharmaceutical companies to develop potent agonists of the STING receptor
74 (Marloyle et al., 2019). We have recently reported the discovery of E7766 (Figure 1), a potent
75 STING agonist that belongs to a novel class of macrocycle-bridged dinucleotides (Endo et al.,
76 2019). In nonclinical studies, E7766 has demonstrated potent antitumor activity by inducing a
77 robust and effective innate and adaptive antitumoral immune response (Huang et al., 2019).
78 Macrocycle-bridged dinucleotides were generally characterized by moderate to high molecular
79 weight (>400), low logP (<1) and pKa of 3-4. Macrocycle-bridged dinucleotides also have low
80 permeability, and as such fall in the Class 3B of the extended clearance classification system
81 (ECCS) (Varma et al., 2015), thus making them potential substrates for hepatic uptake and efflux
82 transporters. Many compounds in this series showed high clearance that was at or exceeded
83 hepatic blood flow and had low volume of distribution. Additionally, the compounds were
84 metabolically stable in rodent and human hepatocytes and liver S9 fraction indicating that
85 metabolism was unlikely the primary clearance pathway. Identifying clearance mechanisms of
86 these novel class compounds in drug discovery is important to predict systemic and target tissue
87 exposure, as well as to predict clinical drug-drug interaction (DDI).

88 The significant clinical implications of inhibiting hepatic uptake transporters such as
89 OATP1B have highlighted the importance of assessing this potential liability for new chemical
90 entities (NCEs) during drug discovery and development (Chen et al., 2018). The US Food and
91 Drug Administration (US FDA) and the European Medicines Agency (EMA) have also issued

92 guidance for the in vitro and in vivo evaluation of the transporter-based DDI (EMA, 2012; FDA,
93 2017). Predicting DDI for substrates of OATP1B1 and OAPT1B3 has recently been described in
94 many reports (Duan et al., 2017; Yoshikado et al., 2018). Physiologically based pharmacokinetic
95 (PBPK) modeling has been recognized to be a powerful tool for PK and DDI predictions of
96 substrates of hepatic uptake transporters as well as drug metabolizing enzymes (Jones et al.,
97 2015; Wang et al., 2017). In addition to predicting DDI, PBPK can also be used in the
98 mechanistic understanding of various rate-limiting and rate-determining processes in the
99 disposition of drugs.

100 E7766 was selected as a suitable model compound for investigating the clearance mechanisms
101 and transporter-mediated DDI propensity of macrocycle-bridged dinucleotide-type STING
102 agonists. A series of nonclinical studies were planned and conducted to 1) assess the major
103 clearance mechanisms in the systemic clearance of E7766; 2) identify the transporters and
104 estimate their relative contributions to the hepatic clearance of E7766, and 3) use the in vitro
105 transporter data and PBPK model framework to prospectively predict the clinical DDI of E7766
106 with OATP1B inhibitor. To best of our knowledge, this is the first report for the identification of
107 hepatobiliary transporters and PBPK modeling-based DDI prediction of therapeutically
108 important and structurally novel macrocycle-bridged dinucleotides. Our data underscores the
109 importance of OATP1B, especially OATP1B3, in determining the systemic hepatic clearance
110 rate and hence the plasma exposure of E7766 and perhaps this class of compounds. Furthermore,
111 our results also show that clinically relevant DDIs leading to changes in plasma exposure can
112 occur if E7766 is coadministered with OATP1B3 inhibitors. The predominant contribution of
113 OATP1B3 to the clearance of E7766 suggests that the plasma exposure to E7766 is less likely to
114 be subjected to inter-individual variability due to polymorphisms in OATP1B1.

116 **Materials and Methods**

117 **Chemicals and reagents**

118 E7766 and the internal standard (IS), ER-001229535 (Lot No. ER-001229535-NH4-011), were
119 synthesized at Eisai Inc. (Andover, MA). Bovine serum albumin solution was purchased from
120 American Tissue Culture Collection (ATCC; Manassas, VA). Estradiol-17 β -glucuronide
121 (E₂17 β G), Rifampicin, and Krebs-Henseleit buffer (KH buffer) were purchased from Sigma-
122 Aldrich (St. Louis, MO). Porcine kidney LLC-PK1 (parental cells were obtained from Discovery
123 Labware, Inc (now Corning Inc., Tewksbury, MA). HEK293-FT cells stably transfected with the
124 vector containing OATP1B1 cDNA or OATP1B3 cDNA, or empty vector were obtained from
125 Solvo Biotechnology (Zeged, Hungary). TransportoCells™ transiently transfected with the
126 vector containing OATP2B1 cDNA or NTCP cDNA, or empty vector were purchased from
127 Corning (NY, USA). The cell culture related reagents were cell culture grade, and were
128 purchased from Thermo Scientific, Inc. (Herndon, VA). All other reagents used in this study
129 were of either analytical or HPLC grade.

130 **Transport studies of E7766 with hepatic Solute Carrier (SLC) transporters**

131 TransportoCells™ (Corning, NY, USA) transiently expressing OATP2B1 or NTCP and the
132 control cells (HEK293 cells transfected with empty vector), and HEK293FT cell line (Solvo
133 Biotechnology, Zeged, Hungary) stably expressing OATP1B1 (HEK293FT-OATP1B1) or
134 OATP1B3 (HEK293FT-OATP1B3) and the control cells (HEK293FT-control; HEK293FT cells
135 transfected with empty vector) were grown in a Dulbecco's modified Eagle's medium fortified
136 with 10% fetal calf serum and 2 mmol/L sodium butyrate (for NTCP only) in a humidified
137 incubator at 37°C and 5% CO₂. Solvo HEK293-FT cells were harvested at 90% confluence and
138 then seeded in poly-D-lysine-coated 24-well 24 h prior to transporter assay while Corning

139 TransportoCells™ were thawed and seeded in poly-D-lysine-coated 96-well 24 h prior to
140 transporter assay. Cellular transport assays were conducted as described previously (Jiang et al.,
141 2015). Briefly, cells were washed twice and pre-incubated with 200 μ L of pre-warmed Krebs-
142 Henseleit (KH) buffer. After pre-incubation, cells were incubated with 3 or 10 μ mol/L of E7766
143 in presence or absence of 100 μ mol/L of inhibitors (Rifamycin SV for OATP2B1, Troglitazone
144 for NTCP, and Rifampicin for OATP1B1 and OATP1B3). The transport reaction was terminated
145 by aspirating the buffer from the wells at designated time. After washing three times with 200 μ L
146 of ice-cold KH buffer, the cells were lysed and the resulting cellular lysates were analyzed by
147 LC-MS/MS.

148 The time-dependent uptake of E7766 with OATP1B1 and OATP1B3 was evaluated to
149 confirm linear uptake condition range of uptake of E7766 (Supplemental Figure 2).
150 Concentration-dependent uptake of E7766 via OATP1B1 and OATP1B3 was examined with a
151 concentration range of 0.25-100 μ mol/L under linear conditions at 5 minutes. All experiments
152 were run in triplicates.

153 **Transport studies of E7766 with hepatic ABC transporters**

154 TransportoCells™ membrane vesicles (Corning, NY, USA) expressing MDR1, BCRP, BSEP, or
155 MRP2, and control vector vesicles (70 μ L) were pre-incubated with vesicle uptake buffer (47
156 mmol/L MOPs-Tris, 65 mmol/L KCl, 7 mmol/L MgCl₂, pH 7.4 for MDR1 and BCRP; 47
157 mmol/L MOPs-Tris, 2.5 mmol/L GSH, 65 mmol/L KCl, 7 mmol/L MgCl₂, pH 7.4 for MRP2;
158 and 10 mmol/L HEPES-Tris, 100 mmol/L KNO₃, 12.5 mmol/L Mg(NO₃)₂, and 50 mmol/L
159 sucrose, pH 7.4 for BSEP) at 37 °C for 10 minutes. The transport was initiated by adding 125 μ L
160 of pre-warmed 25 mmol/L MgATP, 3 μ mol/L of E7766 in the presence or absence of inhibitors
161 (3 μ mol/L of Novobioncin for BCRP, 100 μ mol/L of MK-571 for MRP2, and 20 μ mol/L of

162 Ketoconazole for MDR1 and BSEP). The transport was terminated at designated time by adding
163 200 μ L ice-cold vesicle uptake buffer. The complete content was then rapidly filtrated using
164 multi-screen HTS vacuum manifold, followed by 5 washes and filtrations. The plate was allowed
165 to dry completely and then placed onto a 96-well receiver plate. A 50 μ L of elute solution (75%
166 methanol containing the internal standard) was added into each assay well followed by
167 centrifugation at 2000 rpm for 5 minutes. This lysis-and-centrifugation procedure was repeated
168 one more time to maximize compound extraction. The samples from two centrifugation were
169 combined and analyzed by LC-MS/MS. All experiments were run in triplicates.

170 The LLC-PK1 cell-based permeability of E7766 was also assessed. Porcine kidney LLC-
171 PK1 cells were cultured at 37 °C and 5% CO₂ in Medium 199 containing 10% fetal bovine
172 serum, 292 μ g/mL glutamine, 0.1 mg/mL hygromycin B, and 0.05 mg/mL gentamycin. The cells
173 were seeded in HTS Transwell–96 systems (polystyrene, 4.26 mm in diameter, 0.14 cm² surface
174 area, 1.0 μ m in pore size, Corning Inc. Corning, NY) at a density of approximately 1.4×10^6
175 cells/mL. Culture medium was replaced on the fourth and sixth day after seeding. Cells were
176 cultured for 7 days on Transwell plates for the studies. Prior to the experiments, LLC-PK1 cells
177 were washed using transport buffer (HBSS supplemented with 10 mmol/L HEPES) and
178 incubated for 60 minutes. For the experiments of apical to basolateral (A–B) direction, transport
179 buffer containing 1 μ mol/L of E7766 was added into the apical compartment while transport
180 buffer with the same treatment was added into the basolateral compartment. For the experiments
181 of basolateral to apical (B–A) direction, transport buffer containing 1 μ mol/L of E7766 was
182 added into the basolateral compartment while transport buffer with the same treatment was
183 added into the apical compartment. The length of incubation for transport was 2 hours and
184 samples were stored at –70 °C or lower prior to LC-MS/MS analysis.

185 **Hepatic uptake and biliary excretion of E7766 in sandwich cultured human hepatocytes**
186 **(SCHH)**

187 Transporter Certified™ cryopreserved human hepatocytes (BioIVT, Durham, NC, USA; Donor
188 JEL) were thawed following manufacturer's instructions. Cryopreserved hepatocytes were
189 subsequently suspended in BioIVT proprietary hepatocyte seeding medium (QualGro™ Seeding
190 Medium) and seeded at a density of 0.9 million viable cells/mL onto BioCoat® 24-well cell
191 culture plates (San Jose, CA, USA). Following plating, cells were allowed to attach for 2-4
192 hours, then were rinsed and fed with warm (37°C) seeding medium. Eighteen to 24 hours later,
193 cells were fed and overlaid with QualGro™ culture medium (QTS, Durham, NC, USA)
194 supplemented with extracellular matrix Matrigel® (BD Biosciences, San Jose, CA, USA; 0.25
195 mg·mL⁻¹). Cells were then maintained in QualGro™ Hepatocyte Culture Medium. Hepatic
196 uptake clearance and hepatobiliary disposition of test articles were assessed on day 5 by using B-
197 CLEAR® Technology (Swift, Pfeifer & Brouwer, 2010). Briefly, to assess uptake clearance, cell
198 culture medium was removed, and hepatocytes were washed three times with warm Plus (+)
199 Buffer (0.3 mL per well). Immediately following washing step, dose solutions for E7766 or
200 comparators (0.3 mL per well) were added and incubated for 1, 5, and 10 minutes at 37°C.
201 Following incubation period, the solutions were collected and frozen at -80°C until process for
202 bioanalysis. The wells were then washed three times with ice cold Plus (+) Buffer. The plates
203 were frozen at -80 °C until bioanalysis.

204 To assess biliary clearance, cell culture medium was removed, and hepatocytes were
205 washed twice with warm Plus (+) or Minus (-) Buffer to maintain or disrupt tight junctions,
206 respectively. The wash solutions were removed and replaced with fresh Plus (+) Buffer or
207 Minus (-) Buffer (0.3 mL per well). The hepatocytes were conditioned for 10 minutes at 37 °C.

208 The conditioning solutions were removed and replaced with dosing solutions for E7766 or
209 comparators (0.3 mL per well). Following a 20-minute incubation, the solutions were collected
210 and frozen at -80 °C until process for bioanalysis. The wells were then washed three times with
211 ice cold Plus (+) Buffer. The plates were frozen at -80 °C until processed for bioanalysis. All
212 experiments were run in triplicates.

213 **In vivo Pharmacokinetics**

214 All in vivo study protocols were approved by appropriate Institutional Animal Care and Use
215 Committee. Animals were monitored during the study and provided free access to food and
216 water.

217 **Pharmacokinetics in bile-duct cannulated (BDC) rats and dogs**

218 BDC male Sprague Dawley rats (n=4) and BDC male Beagle dogs (n=3) were given E7766 as a
219 single 1 mg/kg IV dose and 0.075 mg/kg IV dose as free acid prepared in sterile PBS,
220 respectively. Plasma samples were collected at pre-dose and designate time points post-dose via
221 a jugular vein, into tubes containing sodium heparin as the anticoagulant. Urine samples were
222 collected at intervals 0 to 4, 4 to 8, and 8 to 24 hours post-dose into collection tubes on wet ice.
223 Bile and feces (rat only) samples were collected at intervals 0 to 4, 4 to 8, and 8 to 24 hours post-
224 dose into collection tubes on wet ice. All samples were stored at -70 °C or lower until LC-
225 MS/MS analysis.

226 **Pharmacokinetics in humanized OATP1B1/1B3 and wild type (WT) mice**

227 E7766 was formulated in 0.5% 0.1 N HCl, 5% DMSO, 10% EtOH, 84.5% saline for studies in
228 WT and humanized OATP1B1/1B3 mice. Rifampicin was formulated in 0.5% 0.1 N HCl, 5%
229 DMSO, 10% EtOH, 84.5% saline. Age-matched OATP1B1 and OATP1B3-knockin humanized

230 mice (n=3) on the Oatp1a/1b-knockout background, and wild-type (WT) FVB male mice
231 (n=3/timepoint) were purchased from Taconic Biosciences (Hudson, NY, USA). Mice were
232 between 8 and 10 weeks of age (22–34 g) at the time of study. In WT mice, E7766 was
233 administered via the tail vein at a dose of 0.5 mg/kg with either vehicle or Rifampicin (30 mg/kg
234 IV). Plasma and liver samples were collected at 0.083, 0.25, 0.5, 1, 1.5, 3, 6 hours and all
235 samples were stored at -80°C until bioanalysis. In humanized mice, E7766 was administered via
236 the tail vein at a dose of 1 mg/kg or together with vehicle or with Rifampicin (E7766, 0.5 mg/kg;
237 Rifampicin, 10 mg/kg). Blood samples were collected at pre-dose, and 0.08, 0.25, 0.5 1, 1.5, 3, 6
238 and 24 hours post-dose via saphenous or tail vein into a heparinized capillary. The contents of
239 the capillary were expelled onto an appropriate spot on a DBS card (FTA DMPK-B [GE
240 Healthcare, Life Sciences, WhatmanTM]). Urine and feces samples were collected from all dose
241 groups at intervals 0-8 and 8-24 hours post-dose. Samples were stored at -80°C until bioanalysis.

242 **LC-MS/MS analysis**

243 Cell lysates samples were extracted by 70:30 methanol:water (v:v) containing internal standard
244 (IS) 10 nmol/L ER-001229535. Plasma samples were subjected to protein precipitation with
245 methanol containing ER-001229535 as the IS. Urine, bile and feces samples were extracted via
246 salting-out assisted liquid-liquid extraction based on the methodologies described by Tang and
247 Weng, 2013. For analysis of E7766 and IS of ER-001229535, a Shimadzu HPLC system
248 (Shimadzu Scientific Instruments, Columbia, MD), which consisted of an autosampler (model:
249 SIL HTc), a column compartment unit (model: CTO-20AC), a degasser (model: DGU-20A3),
250 two pumps (model: LC-20AD), and a high pressure switching valve (model: FCV-20AH6) was
251 used. The mobile phase A consisted of 2 mmol/L ammonium bicarbonate in H₂O/MeOH (95/5,
252 v/v), and mobile phase B consisted of 2 mmol/L ammonium bicarbonate in MeOH/H₂O (95/5,

253 v/v). Aliquots (10 μ L) were injected onto a Waters XBridge Oligonucleotide BEH C18 column,
254 130 \AA , 2.5 μ m (4.6 mm inner diameter \times 50 mm length) at a flow rate of 0.5 mL/min at 40 $^{\circ}$ C.
255 The temperature of the autosampler was controlled at 4 $^{\circ}$ C. The samples were analyzed on an
256 API5000 (Sciex, Framingham, MA) triple quadrupole mass spectrometer with turbospray
257 ionization (ESI) under negative ion mode. A 9 min gradient was run for E7766 and IS, with a
258 flow rate of 0.5 mL/min as follows: 0% B for 0.3 min, 0% to 100% B over 2.7 min, 100% B for
259 2 min, 100% to 0% B over 0.2 min, then re-equilibration at 0% B for 3.8 min. Analytes were
260 detected by multiple reaction monitoring (MRM) by the following mass transitions: 372.4 (M-
261 2H) $^{2-}$ >186.5 for E7766 (-38 eV collisions) and 689.3 (M-H) $^{-}$ >134.1 for IS (-75 eV collisions).

262 **PBPK model and DDI simulations**

263 Whole-body PBPK modeling and simulation were performed using the population-based
264 absorption, distribution, metabolism, and excretion simulator, SimcypTM (version 18, Certara,
265 Sheffield, UK). Each simulation was performed for 100 subjects (10 trials \times 10 subjects) using
266 the software's built-in healthy volunteer virtual population. To simulate the effect of OATP
267 inhibitors on the PK of E7766, the PBPK model for Rifampicin-SD was adopted directly from
268 the default SimcypTM compound library. For all simulations, E7766 was administered as a single
269 intravenous dose and Rifampicin was administered as a single oral dose. Physicochemical
270 properties and input parameters for E7766 used for the PBPK model are summarized in Table 4.
271 Parameters of Rifampicin for the DDI simulation are summarized in Supplemental Table 4

272 The full-PBPK model with Method 2 (based on Rodgers and Rowland) was used to
273 predict the volume of distribution (V_d) of E7766 (Rodgers et al., 2005; Rodgers and Rowland,
274 2006). A K_p scalar of 4 was applied to the prediction of human V_d . The K_p scalar was determined
275 based on the predicted versus observed V_d of E7766 in preclinical species. Permeability-limited

276 disposition was considered for liver. The DDI simulation was run in two scenarios: 1) Hepatic
277 uptake clearance was assigned from the transporter kinetics (V_{\max}/K_m) for OATP1B1 and
278 OATP1B3 measured in the HEK293FT system, and intrinsic passive diffusion across the
279 sinusoidal membrane measured in SCHH studies, and scenario 2) intrinsic active uptake
280 clearance, passive clearance on the sinusoidal membrane and efflux clearance on the canalicular
281 membrane, measured in the SCHH studies, were used to capture hepatobiliary disposition. In
282 both scenarios, the intrinsic uptake clearances were scaled up to physiologically relevant uptake
283 clearance by a relative expression factor (REF) approach (Hirano et al., 2004) within Simcyp
284 models. Additionally, in second scenario, the intrinsic uptake clearance from SCHH was
285 assigned to OATP1B3 ($f_t = 0.97$) to capture the DDI. Based on in vitro metabolism data using
286 cryopreserved human hepatocytes (data not shown), metabolic clearance was assumed to be
287 negligible for both simulations. PK in preclinical studies suggest that E7766 is expected to be
288 eliminated from kidney via glomerular filtration. The renal clearance of E7766 was then fixed as
289 3 L/h as a product of GFR (~6 L/h in human; Lin et al. 2003) and plasma protein binding of
290 E7766 (0.5, measured data, Table 4). This fixed renal clearance also aligned well with back
291 calculation from systemic clearance and the observation from PK studies of multiple preclinical
292 species, where about 10% of E7766 was excreted in urine as parent compound. Sensitivity
293 analysis was performed to evaluate changes in drug exposure and DDI due to any uncertainty in
294 the in vitro parameters.

295 **Data analysis**

296 The uptake velocity describes the rate of E7766 taken up by active and/or passive processes of
297 the transporter-expressing cell or vesicles, and is calculated as follows:

$$298 \quad \text{uptake velocity} = (C \times V)/T/W \quad (1)$$

299 where C represents the concentration of E7766 in the cellular (or vesicular) lysate ($\mu\text{mol/L}$), V is
300 the volume of the lysate (μL), T is the incubation time and W is the measured cellular (or
301 vesicular) protein amount of each well (mg).

302 The OATP1B1 or OATP1B3 specific uptake velocity was calculated by subtracting mean uptake
303 velocity of E7766 in HEK293-Control cells from that of HEK293FT-OATP1B1 or HEK293FT-
304 OATP1B3 cells at each of the corresponding concentration. Kinetic and statistical analyses of the
305 transport data were conducted using GraphPad Prism Ver. 7.02 (GraphPad Software, Inc., San
306 Diego, CA). Kinetic data was fit to a Michaelis-Menten model as follows:

$$307 \quad v = V_{max} \times S/[K_m + S] \quad (2)$$

308 where v is the OATP1B1 or OATP1B3 specific uptake velocity (pmol/mL/mg protein), S is the
309 concentration of E7766 in the uptake buffer ($\mu\text{mol/L}$), K_m is the apparent Michaelis-Menten
310 constant ($\mu\text{mol/L}$), and V_{max} is the apparent maximum uptake rate (pmol/min/mg protein). The in
311 vitro intrinsic clearance ($CL_{\text{int, in vitro}}$) was calculated as follows:

$$312 \quad CL_{\text{int, in vitro}} = V_{max}/K_m \quad (3)$$

313 The relative contribution of OATP1B1 and OATP1B3 to the hepatic uptake of E7766 was
314 assessed by the relative expression factor (REF) approach (Kunze et al., 2014). REF for each
315 transporter was calculated by following equations:

$$316 \quad REF_{1B1} = \frac{EXP_{\text{OATP1B1, HEP}}}{EXP_{\text{OATP1B1, HEK}}} \quad (4)$$

$$318 \quad REF_{1B3} = \frac{EXP_{\text{OATP1B3, HEP}}}{EXP_{\text{OATP1B3, HEK}}} \quad (5)$$

320 where EXP represents the specific transporter expression (fmol/mg protein) determined in
321 primary human hepatocyte (HEP), or HEK293FT-OATP1B1 or HEK293FT-OATP1B3 cell line

322 (HEK). The expression levels of OAPT1B1 and OATP1B3 in hepatocyte and HEK293-FT
323 overexpressing cell line are summarized in Supplemental Table 2.

324 For SCHH assays, the intrinsic hepatic uptake clearance (Liver Uptake $CL_{int,T}$) was determined
325 using following:

$$326 \quad \text{Uptake } CL_{int,T} = A_{\text{Plus (+)Buffer}} / (T \times C_{\text{initial}}) \quad (6)$$

327 where $A_{\text{Plus (+)Buffer}}$ is the total accumulation of E7766 (cells + bile pocket) in SCHH after
328 incubation with Plus (+) buffer (μmol), T is the incubation time (min), and C_{initial} is the initial
329 concentration of E7766 in dosing medium ($\mu\text{mol/L}$).

330 The biliary excretion index (BEI) was obtained from equation 7 and intrinsic biliary clearance
331 (Liver Efflux $CL_{int,T}$) was calculated from equation 8:

$$332 \quad \text{BEI} = 100 \times [A_{\text{Plus (+)Buffer}} - A_{\text{Minus(-)Buffer}}] / A_{\text{Plus (+)Buffer}}$$

333 (7)

$$334 \quad \text{Efflux } CL_{int,T} = [A_{\text{Plus (+)Buffer}} - A_{\text{Minus(-)Buffer}}] / (T \times C_{\text{initial}}) \quad (8)$$

335 where $A_{\text{Minus(-)Buffer}}$ is cellular accumulation inside hepatocytes (cells only) after incubation with
336 Minus (-) buffer (μmol).

337 PK parameters of E7766 were obtained by non-compartmental analysis using Phoenix
338 WinNonlin® Ver. 7.0.0.2535 (Certara USA, Inc., Princeton, NJ, USA). The parameters
339 calculated were the cumulative amount of E7766 recovered in urine ($X_{u(0-t)}$), bile ($X_{b(0-t)}$) and
340 feces ($X_{f(0-t)}$), which were determined as the sum of the amounts recovered in each sampling
341 interval; the percent of the administered dose excreted in urine ($A_{e \text{ renal}} \%$), bile ($A_{e \text{ biliary}} \%$) and
342 feces ($A_{e \text{ fecal}} \%$); and the renal (CL_{renal}), biliary (CL_{biliary}) and fecal clearances (CL_{fecal}), which
343 were calculated using the cumulative amount recovered up to the last measurable urine, bile, or
344 feces sample along with the $AUC_{(0-t, \text{last})}$ as $CL_{\text{renal}} = X_{u(0-t, \text{last})} / AUC_{(0-t, \text{last})} / \text{body weight}$,

345 $CL_{\text{biliary}} = Xb_{(0-t, \text{ last})} / AUC_{(0-t, \text{ last})} / \text{body weight}$ and $CL_{\text{fecal}} = Xf_{(0-t, \text{ last})} / AUC_{(0-t, \text{ last})} / \text{body}$
346 weight, respectively.

347

348 **Results**

349 **Assessment of E7766 as a substrate of hepatic uptake transporters**

350 As shown in Figure 2A, OATP1B1 and OATP1B3 showed significant active uptake of E7766
351 ($p < 0.000001$ and $p = 0.000021$ for OATP1B1 and OATP1B3, respectively), which could be
352 inhibited by Rifampicin (100 $\mu\text{mol/L}$; $p < 0.000001$ and $p = 0.000007$ for OATP1B1 and
353 OATP1B3, respectively). Active uptake of E7766 was not observed in cells expressing
354 OATP2B1 ($p = 0.11$) or NTCP ($p = 0.11$). The results indicated that E7766 is a substrate for
355 OATP1B1 and OATP1B3 but not a substrate for OATP2B1 and NTCP. We observed differences
356 in passive uptake of E7766 with mock cells groups and this was at least partially due to the
357 differences in cell subtypes, cell engineering, culture conditions and assay conditions.
358 Additionally, very low passive permeability of E7766 could add further variability of passive
359 uptake with mock cells. To support the validation of in vitro assay systems, uptake activity of
360 positive control substrates was summarized in Supplemental Figure 1A.

361 The results of concentration-dependent uptake of E7766 in HEK293FT-OATP1B1,
362 HEK293FT-OATP1B3, and HEK293FT-Control cells are summarized in Figure 3. The data
363 were best-fitted to a Michaelis-Menten model, and the kinetic parameters for uptake of E7766 by
364 OATP1B1 were calculated as 2.2 $\mu\text{mol/L}$ (K_m) and 27.8 $\text{pmol/min/mg protein}$ (V_{max}). The in
365 vitro uptake clearance ($\text{CL}_{\text{int, in vitro}}$) of OATP1B1 was then calculated to be 12.6 $\mu\text{L/min/mg}$
366 protein. The K_m , V_{max} , and $\text{CL}_{\text{int, in vitro}}$ of OATP1B3-mediated uptake of E7766 were estimated as
367 4.0 $\mu\text{mol/L}$, 81.3 $\text{pmol/min/mg protein}$, and 20.5 $\mu\text{L/min/mg protein}$, respectively. The relative
368 expression factors (REFs) for OATP1B1 and OATP1B3 were calculated to be 0.1 and 2.8,
369 respectively using the measured expression of these transporters in the overexpressing cell lines
370 and the reported expression levels in human hepatocytes from Schaefer et.al, 2012

371 (Supplemental Table 2). We decided to use the transporter expression reported by Schaefer et.al,
372 2012 because the methodology used to extract the membrane protein and measure the protein
373 content aligned with the methodology used to measure transporter expression in our HEK293FT
374 overexpressing system.

375 **Assessment of E7766 as a substrate of biliary efflux transporters**

376 E7766 was incubated with either MDR1, BCRP, BSEP or MRP2 expressing or control vesicle
377 membranes. As shown in Figure 2B, E7766 did not show transporter-mediated uptake activities
378 in MDR1 ($p>0.99$), BCRP ($p=0.17$) and BSEP ($p=0.45$) expressing vesicles. Incubation of
379 E7766 with MRP2-expressing vesicles resulted in greater uptake activity than that with control
380 vesicles with an uptake ratio of 23 and a p -value of 0.00014. Co-incubation of E7766 and
381 positive control inhibitor MK-571 (100 $\mu\text{mol/L}$) with MRP2 expressing vesicles, decreased the
382 uptake ratio from 23 to 1.1 ($p=0.00014$). The results indicated that E7766 is a substrate of efflux
383 transporter MRP2, but not a substrate of MDR1, BCRP or BSEP (Figure 2B). The transporter
384 activity of positive control substrates for MDR1, MRP2, BCRP and BSEP is shown in
385 Supplemental Figure 1B. The transcellular permeability of E7766 was assessed in LLC-PK1
386 cells. The results, as shown in Supplemental Table 1 indicated that E7766 exhibited very low
387 permeability in LLC-PK1 cells ($P_{\text{app}} < 1 \times 10^{-6}$ cm/s).

388 **Evaluation of hepatic uptake and biliary excretion of E7766 in SCHH**

389 The transporter-mediated hepatic uptake potential of E7766 was evaluated in SCHH prepared
390 from one donor (JEL). The intrinsic hepatic uptake clearance of E7766 (uptake $CL_{\text{int,T}}$) at 4 °C
391 was markedly decreased to <7.6% of that at 37 °C at two lower dose levels (0.3 and 1.0 $\mu\text{mol/L}$)
392 (Table 1). The uptake $CL_{\text{int,T}}$ of E7766 across all dose levels dropped rapidly from 1 to 5 minutes
393 (Table 1). These results suggested hepatic uptake was rapidly achieving near maximal

394 accumulation within 5 minutes. In addition, the uptake $CL_{int,T}$ decreased dramatically at 10
395 $\mu\text{mol/L}$ across all exposure periods compared to uptake $CL_{int,T}$ measured at 0.1 $\mu\text{mol/L}$ and 3
396 $\mu\text{mol/L}$ suggesting hepatic uptake was saturated at concentration of $>1.0 \mu\text{mol/L}$ (Table 1). Taken
397 together, these results suggested that hepatic uptake of E7766 was primarily mediated by a
398 relatively fast active uptake mechanism.

399 As shown in Table 1, following 20-minute exposure, the intrinsic biliary efflux clearance
400 (efflux $CL_{int,T}$) decreased dramatically at 10 $\mu\text{mol/L}$ compared to those at doses of 0.3 and 1
401 $\mu\text{mol/L}$ suggesting hepatobiliary transport of E7766 was saturated at concentration of >1.0
402 $\mu\text{mol/L}$. The BEI of E7766 ranged from 70.9 to 86.2% across the concentration range assessed.
403 These BEI values were comparable to d8-TCA (72.6%), a model bile acid, and was ~ 2 -fold
404 greater than the reference compound rosuvastatin (BEI = 42.7%). The difference in BEI for
405 Rosuvastatin and d8-TCA/E7766 are likely due to differences in uptake and efflux mechanisms
406 as well as kinetics of uptake and efflux of these compounds in the SCHH system. Overall, these
407 results suggested the biliary excretion of E7766 is mediated by a saturable mechanism and with a
408 relatively high BEI value.

409 **Pharmacokinetics of E7766 in bile-duct cannulated BDC rats and dogs**

410 The PK of E7766 in BDC rats (Table 2) was characterized by high $CL_{tot,p}$ (6.50 L/h/kg) and
411 moderate V_{ss} (2.47 L/kg). The mean $X_{u(0-t)}$ and $X_{b(0-t)}$ up to 24 hours postdose were 38,600 and
412 261,000 ng, respectively, which corresponds to 13.7% ($A_{e \text{ renal}}$) and 92.1% ($A_{e \text{ biliary}}$) of the total
413 dose administered, respectively. The mean cumulative amount of E7766 excreted in feces ($X_{f(0-t)}$)
414 up to 24 hours postdose was 991 ng, which correspond to 0.4% of the total dose administered ($A_{e \text{ fecal}}$). Mean CL_{renal} , CL_{biliary} and CL_{fecal} of E7766 in BDC rats were 0.895 L/h/kg, 6.04 L/h/kg and
415 0.0227 L/h/kg, respectively.

417 The PK of E7766 in BDC dogs (Table 2) was characterized by moderate total plasma
418 clearance ($CL_{tot,p}$, 1.29 L/h/kg) and limited volume of distribution (V_{ss} , 0.553 L/kg). The mean
419 cumulative amounts of unchanged E7766 excreted in urine ($Xu_{(0-t)}$) and bile ($Xb_{(0-t)}$) up to
420 48 hours postdose were 33,400 and 625,000 ng, respectively, which correspond to 5.0% ($A_{e\ renal}$)
421 and 87.9% ($A_{e\ biliary}$) of the total dose administered, respectively. Mean renal (CL_{renal}) and biliary
422 ($CL_{biliary}$) clearances of E7766 in dogs were 0.0528 L/h/kg and 1.19 L/h/kg, respectively.

423 **Pharmacokinetics of E7766 in OATP1B1/1B3 humanized and wild type (WT) mice**

424 The plasma and liver PK of E7766 in WT mice was assessed with or without coadministration of
425 Rifampicin (Figure 4). The unbound concentration-time profiles of Rifampin in wild type and
426 humanized mice are shown in Supplemental Figure 3. The plasma PK of E7766 in WT was
427 characterized by high $CL_{tot,p}$ (8.93 L/h/kg) and moderate V_{ss} (1.66 L/kg) (Table 3). In the
428 presence of Rifampicin, the plasma exposure (AUC_{total}) of E7766 in WT mice increased 5.4-fold
429 with a corresponding decrease in $CL_{tot,p}$. The liver exposure to E7766 was comparable in WT
430 mice with or without coadministration of Rifampicin indicating that Rifampicin only affects the
431 plasma exposure and that liver exposure is unchanged by Rifampicin. However, the liver-to-
432 plasma ratio $K_{p,total}$ of E7766 in Rifampicin treated animals decreased by 82% indicating a strong
433 inhibition of Oatp mediated hepatic uptake of E7766 in mice (Table 3). The dose normalized
434 plasma exposure ($AUC_{total}/Dose$) and $CL_{tot,p}$ were compared between WT mice ($AUC_{total}/Dose$:
435 112 ng/h/mL⁻¹/[mg/kg] and $CL_{tot,p}$: 8.93 L/h/kg) and OATP1B1/1B3 humanized mice
436 ($AUC_{total}/Dose$: 126 ng/h/mL⁻¹/[mg/kg] and $CL_{tot,p}$: 9.20 L/h/kg). The dose normalized AUC in
437 humanized mice increased 4.8-fold after coadministration with Rifampicin, which aligned with
438 the increase in AUC (5.4-fold) in WT mice. We also assessed the percentage of the E7766 dose
439 excreted in the urine and feces in the above studies (Figure 4). The dose excreted in the feces in

440 both WT and OATP1B1/1B3 humanized mice decreased to a similar extent (3-fold lower in WT
441 mice and 4.6-fold lower in humanized mice) in the presence of Rifampicin. This decrease is in
442 line with the corresponding increase in systemic exposure to E7766 in the presence of
443 Rifampicin.

444 **PBPK modeling and DDI simulation of E7766**

445 The predicted plasma PK and systemic clearance as well as AUC ratio of E7766 in the presence
446 and absence of Rifampicin are presented in Figure 5 and Table 5. In scenario one of the DDI
447 simulation, active uptake clearances measured as J_{\max}/K_m in HEK293 cells were assigned to
448 OATP1B1 and OATP1B3, and the passive sinusoidal and biliary efflux clearances were taken
449 from the SCHH experiment. Based on the REF factor and the in vitro uptake kinetics, the f_t for
450 OATP1B3 and OATP1B1 were predicted to be 0.97 and 0.02, respectively, thus suggesting that
451 OATP1B3 plays a predominant role in the hepatic uptake of E7766 (Figure 5A). The
452 contribution of passive sinusoidal diffusion clearance to the overall uptake CL of E7766 was
453 negligible (1%, Figure 5A). This simulation showed that the plasma AUC_{total} increases by 2.77-
454 fold whereas the C_{\max} in the presence of Rifampicin is unchanged (Figure 5B). The free liver
455 intracellular C_{\max} of E7766 in the presence of Rifampicin decreases by 31.1% and E7766
456 concentration further decreases to 72.6% at 1 hour after dosing due to impairment of OATP1B
457 function. However, as shown in Figure 5C after 1 hour, the liver intracellular concentration starts
458 to increase at later time points and therefore results in an unchanged liver intracellular AUC_{free}
459 (69.06 nmoL/h/L, Table 5) in presence of Rifampicin compared to Rifampicin free group (76.19
460 nmoL/h/L, Table 5). This increase of liver concentrations at later time points is due an increase in
461 the systemic exposure of E7766 in the presence of Rifampicin. A sensitivity analysis was
462 performed for the in vitro parameters with uncertainty. As shown in Figure 5D-F, the change in

463 AUC ratio ranged from 1.0 to 2.6 when the REF or kinetic parameters for OATP1B3 were
464 varied. The AUC ratio remained unchanged when the REF or kinetic parameters for OATP1B1
465 was varied indicating that the DDI was not sensitive to changes in J_{\max} , K_m and REF for
466 OATP1B1. It is noteworthy that, AUC ratio first increases along with the increase of OATP1B3
467 REF (when OATP1B3 REF < 3) and then starts to drop as OATP1B3 REF increased further until
468 AUC ratio becomes ultimately close to unity (Figure 5D). One potential reason for this pattern
469 maybe that, the hepatic uptake clearance increases when the OATP1B3 REF increased and will
470 result in a larger DDI magnitude, i.e., a greater AUCR in the beginning when REF is in a
471 relatively low range. However, as the OATP1B3 REF increases further (above three), the
472 intrinsic uptake clearance will exceed hepatic blood flow and become a blood-flow rate limited
473 process. Therefore the AUC is not readily affected by inhibition of uptake clearance. We
474 speculate that another explanation may be that E7766 is being cleared away from the transporter
475 binding site very rapidly when REF increases further. Thus there is not enough duration of
476 exposure for E7766 (given as i.v. bolus dose) to have interaction with orally administered
477 Rifampicin, which needs time to get to the interaction site in liver.

478 In the second scenario, DDI was simulated using active uptake, passive sinusoidal uptake
479 and biliary efflux clearances measured in SCHH experiment. In this simulation, we observed
480 similar results for both PK profile and DDI potential of E7766 as victim compared to the first
481 scenario. The comparison between two different scenarios are summarized in Table 5. Simulation
482 showed that the plasma AUC increases by 2.59-fold whereas the C_{\max} in the presence of
483 Rifampicin is unchanged. The liver AUC_{free} calculated by free intracellular concentrations
484 remained unchanged in the presence of Rifampicin with a liver AUC_{free} ratio of 0.86. The

485 consistency of prediction from two scenarios which adopted experimental data from two
486 independent approaches suggests that the PBPK model is mechanistically sound.

487

488 **Discussion**

489 E7766 is a macrocycle-bridged dinucleotide under development as an immuno-oncology drug to
490 be used as a single agent or in combination with other standard of care therapies. For several
491 drugs such as pravastatin which are cleared primarily via biliary excretion, hepatic uptake is in
492 fact the rate limiting step (Nakai et al., 2001), and inhibition of these uptake processes or
493 polymorphisms in the hepatic uptake transporters may lead to clinically relevant change in the
494 PK of drugs (Chen et al., 2018). Therefore, in vitro and in vivo studies were conducted for
495 E7766 to systemically investigate drug transporters involved in its systemic clearance and to
496 predict clinical DDI potential using PBPK models.

497 PK and excretion studies of E7766 were first conducted using BDC rats and BDC dogs.
498 The results confirmed that biliary excretion plays predominant role in systemic clearance of
499 E7766. To further study the clearance mechanisms of E7766, DDI studies with Rifampicin were
500 conducted with OATP1B1/1B3 humanized and WT mice. Coadministration with Rifampicin in
501 OATP1B1/1B3 humanized mice as well as WT mice resulted in an approximately 5-fold
502 decrease in plasma clearance of E7766. We also measured the liver exposure of E7766 with and
503 without coadministration with Rifampicin in WT mice. While liver AUC was comparable
504 between mice with or without Rifampicin, the observed decrease in liver/plasma ratio (liver
505 $K_{p,total}$) in WT mice in the presence of Rifampicin is consistent with hepatic OATP-mediated
506 uptake. Studies in bile-duct cannulated dogs and rats show that biliary excretion of unchanged
507 drug is the major route of clearance in preclinical species. Fecal excretion of unchanged drug
508 was also observed in humanized and WT animals and excretion into the feces decreased
509 substantially in animals where liver OATP/oatp function was inhibited. Taken together these
510 results suggest that E7766 is cleared from systemic circulation primarily via active uptake into

511 the liver by OATP/oatp and then excreted unchanged into the bile. Previous reports have shown
512 that hepatic expression of OATP1B1 in the humanized mice was lower than in human liver
513 whereas the expression of OATP1B3 was 3-fold higher than in human liver (Higgins et al.,
514 2014). These differences in the expression could lead to the overestimation of the contribution of
515 OATP1B3 on the systemic exposure of OATP substrates in humanized mice. However,
516 OATP1B1/1B3 humanized mice may still be useful in qualitatively determining whether hepatic
517 OATP can impact systemic exposure and hepatic distribution of substrates.

518 To prospectively predict clinical DDI potential for E7766 as the victim drug, we used in
519 vitro kinetic data generated from transporter overexpressing cell lines coupled with REF
520 approach (scenario one) and Cl_{int} data from SCHH coupled with REF approach (scenario two) to
521 build “bottom-up” full PBPK models and run DDI simulations. DDI simulation with Rifampicin
522 suggests that Rifampicin may cause about 2-3 fold increase in plasma AUC in both scenarios,
523 indicating that the current PBPK model is mechanistically sound. Similar to the findings in mice
524 treated with Rifampicin, PBPK simulation showed that the intracellular free liver AUC did not
525 change with treatment with Rifampicin, however the liver-to-plasma ratio decreased in the
526 presence of Rifampicin. Previously reported PBPK approaches suggested the need for empirical
527 scaling factors for hepatic active uptake to recover human PK of several OATP substrates (Jones
528 et al., 2012; Watanabe, et al.,2009). These scaling factors are derived from “top down”
529 approaches and are often compound specific (Varma et al., 2013). Hence the model developed
530 here will need to be verified and E7766 specific scaling factors will be derived once clinical PK
531 and DDI data for E7766 are available.

532 For prospective DDI assessment, a sensitivity analysis of parameters that have high
533 uncertainty is important. For transporter-mediated DDIs, there is significant uncertainty due to

534 the limited understanding of quantitative translation of in vitro transporter kinetics to the clinical
535 scenario. Hence we conducted a sensitivity analysis of the in vitro J_{\max} , K_m and REF values. The
536 sensitivity analysis results showed that AUC ratio is less sensitive to changes in the kinetic
537 parameters for OATP1B1 than those of OATP1B3 due to predominant role of OATP1B3 in the
538 overall clearance. On the other hand, based on f_i of E7766 for OATP1B1 and the sensitivity
539 analysis, we can conclude that the pharmacokinetics of E7766 is less likely to be influenced by
540 polymorphisms in OATP1B1. While the impact of genetic polymorphisms of OATP1B1 on the
541 PK/PD of OATP1B substrates has been well documented (Niemi et al., 2011), that of OATP1B3
542 polymorphisms has not been clearly reported. Reduced uptake of glibenclimide and glipizide by
543 OATP1B3 in HEK cells expressing OATP1B3 (699G > A) was recently reported (Yang et al,
544 2018). However, there are no reported clinical studies to support these in vitro observations. It is
545 however advisable to genotype patients and healthy volunteers for any potential OATP1B3
546 polymorphisms to understand any inter-individual variability in E7766 exposure.

547 E7766 was also identified as a novel substrate of MRP2, an efflux transporter expressed
548 on the canalicular membrane of human hepatocytes. MRP2 is essential for hepatobiliary and
549 renal elimination of many anionic substrates, including drugs and conjugates such as bilirubin
550 glucuronides (Nies and Keppler, 2007). It was reported that Rifampicin when dosed 600 mg
551 orally may inhibit MRP2-mediated biliary excretion of (15R)-¹¹C-TIC-Me (Takashima et al.,
552 2012). However, it is likely that the OATP mediated uptake rather than MRP2 mediated efflux
553 influences the systemic exposure of E7766. This conclusion is based on, 1) ECCS classification
554 which states that hepatic uptake will be the major contributor to the clearance of class 3B
555 compounds and, 2) Others reported (Watanabe, et al., 2009) that the impairment of MRP2 would
556 only affect the liver AUC but has no impact on plasma AUC if the compound is uptake limited.

557 To the best of our knowledge, no systemic DDI has been attributed to MRP2, and there is no
558 evidence that MRP3 or MRP4 should be examined or that there is a likelihood of DDI for a
559 substrate of MRP2 (Hillgren et al., 2013).

560 Further studies are warranted to investigate whether other dinucleotide NCEs are also
561 substrates of OATP1Bs and MRP2. A recent paper published by Luteijn and coworkers (Luteijn
562 et al., 2019) identified SLC19A1 (folate–organic phosphate antiporter) as the major transporter
563 to facilitate cellular uptake of cyclic dinucleotides such as 2'3'-cGAMP into THP-1 cells and
564 therefore has implications for the immunotherapeutic treatment of cancer. The uptake of 2'3'-
565 cGAMP was inhibited by methotrexate and sulfasalazine, inhibitors of SLC transporters.
566 OATP1B1, OATP1B3 and other OATP transporters are also found in multiple cancer cells
567 including breast cancer, colon cancer, liver cancer, pancreatic cancer, prostate cancer, testicular
568 cancer, and thyroid cancer (Pressler et al., 2011; Wlcek et al., 2008). Given that cellular
569 permeability of E7766 or its analogs could be low due to their physiochemical properties,
570 additional investigation into whether other analogs of E7766 are substrates of OATP1B1/1B3,
571 SLC19A1 or other OATP transporters expressed in hepatocytes, immune cells or cancer cells can
572 provide insight into ADME properties and pharmacological function of these novel NCEs.

573 In summary, our data show that transporter-mediated hepatic uptake is the major
574 contributor to the overall systemic clearance of E7766. Based on the estimated f_i for OATP1B3
575 and OATP1B1 we conclude that OATP1B3 plays a predominant role in the hepatic uptake of
576 E7766. The findings reported here have a significant influence on the design of clinical
577 pharmacology program for E7766. Due to near complete recovery of unchanged E7766 observed
578 in preclinical animal studies, the clinical protocols emphasized the need for collecting urine and
579 fecal samples from patient volunteers in Phase I studies to measure the recovery of E7766 in

580 early clinical studies, which will give us useful information about renal and biliary clearances of
581 E7766 in humans. This information could help design an appropriate human ADME study and
582 accelerate clinical development of E7766. Since nonclinical studies have identified transporters
583 responsible for clearance of E7766, appropriate clinical DDI studies can be designed and the
584 PBPK model developed here can be used to predict DDI with perpetrators or co-administered
585 therapies. Finally, the results collected from current studies may also shed light on
586 pharmacokinetics and pharmacodynamics of other compounds from this class of macrocycle-
587 bridged dinucleotides.

588 **Acknowledgements**

589 The authors would like to thank Kazutomi Kusano, Takafumi Komori, Yoshitane Nozaki, Naomi
590 Wakayama, Saki Izumi and Raku Shinkyō from Eisai Co. LTD., Tsukuba, Japan for review and
591 helpful scientific discussions during the preparation of this manuscript.

592 **Authorship Contributions**

593 Participated in research design: Jiang, Dixit, Hart, Lai

594 Conducted Experiments: Jiang, Hart, Burgess

595 Contributed new reagents or analytic tools: Kim

596 Performed Data analysis: Jiang, Dixit, Hart

597 Wrote or contributed to the writing of the manuscript: Jiang, Dixit

598

599 **References**

- 600 Chen Y, Zhu R, Ma F, Mao J, Chen EC, Choo EF, Sahasranaman S and Liu L (2018) Assessment of
601 OATP transporter-mediated drug-drug interaction using physiologically-based pharmacokinetic (PBPK)
602 modeling - a case example. *Biopharm Drug Dispos* 39: 420-430.
- 603 Corrales L, McWhirter SM, Dubensky TW, Jr. and Gajewski TF (2016) The host STING pathway at the
604 interface of cancer and immunity. *J Clin Invest* 126: 2404-2411.
- 605 Duan P, Zhao P and Zhang L (2017) Physiologically Based Pharmacokinetic (PBPK) Modeling of
606 Pitavastatin and Atorvastatin to Predict Drug-Drug Interactions (DDIs). *Eur J Drug Metab*
607 *Pharmacokinet* 42: 689-705.
- 608 EMA (2012) Guideline on the investigation of drug interactions.
- 609 Endo A, Kim DS, Huang KC, Hao M, Mathieu S, Choi HW, Majumder U, Zhu X, Shen Y, Sanders K,
610 Noland T, Chandra D, Chen Y, Tendyke K, Loiacono K, Kolber-Simonds D, Jiang R, Dixit V, Hutz J,
611 Wang J, Bao X, Fang F and Sarwar N (2019) Discovery of E7766: A representative of a novel class of
612 macrocycle-bridged STING agonists (MBSAs) with superior potency and pan-genotypic activity. *Cancer*
613 *Res* 79: Abstract nr 4456.
- 614 FDA (2017) In Vitro Metabolism- and Transporter- Mediated Drug-Drug Interaction Studies Guidance
615 for Industry
- 616 Higgins JW, Bao JQ, Ke AB, Manro JR, Fallon JK, Smith PC and Zamek-Gliszczynski MJ(2014) Utility
617 of Oatp1a/1b-knockout and OATP1B1/3-humanized mice in the study of OATP-mediated
618 pharmacokinetics and tissue distribution: case studies with pravastatin, atorvastatin, simvastatin, and
619 carboxydichlorofluorescein. *Drug Metab Dispos* 42: 182-192.
- 620 Hillgren KM, Keppler D, Zur AA, Giacomini KM, Stieger B, Cass CE, Zhang L and International
621 Transporter Consortium (2013) Emerging transporters of clinical importance: an update from the
622 International Transporter Consortium. *Clin Pharmacol Ther* 94: 52-63.

- 623 Hirano M, Maeda K, Shitara Y and Sugiyama Y (2004) Contribution of OATP2 (OATP1B1) and OATP8
624 (OATP1B3) to the hepatic uptake of pitavastatin in humans. *J Pharmacol Exp Ther* 311:139-146.
- 625 Jiang R, Dong J, Li X, Du F, Jia W, Xu F, Wang F, Yang J, Niu W and Li C (2015) Molecular
626 mechanisms governing different pharmacokinetics of ginsenosides and potential for ginsenoside-
627 perpetrated herb-drug interactions on OATP1B3. *Br J Pharmacol* 172: 1059-1073.
- 628 Jones HM, Barton HA, Lai Y, Bi YA, Kimoto E, Kempshall S, Tate SC, EI-Kattan A, Houston JB,
629 Galetin A and Fenner KS (2012) Mechanistic pharmacokinetic modeling for the prediction of transporter-
630 mediated disposition in humans from sandwich culture human hepatocyte data. *Drug Metab Dispos* 40:
631 1007-1017.
- 632 Jones HM, Chen Y, Gibson C, Heimbach T, Parrott N, Peters SA, Snoeys J, Upreti VV, Zheng M and
633 Hall SD (2015) Physiologically based pharmacokinetic modeling in drug discovery and development: a
634 pharmaceutical industry perspective. *Clin Pharmacol Ther* 97: 247-262.
- 635 Huang KC, McGrath S, Chandra D, Wu J, Kim DS, Albu D, Ingersoll C, Tendyke K, Loiacono K,
636 Noland T, Verbel D, Zhang C, Hao MH, Matijevic M, Dixit V, Hukkanen RR, Hutz J, Wang J, Fang F,
637 Bao X, Kolber-Simonds D, Akram M and Sarwar N.(2019) Discovery and characterization of E7766, a
638 novel macrocycle-bridged STING agonist with pan-genotypic and potent antitumor activity through
639 intravesical and intratumoral administration. *Cancer Res* 79: Abstract nr 3269.
- 640 Kunze A, Huwyler J, Camenisch G and Poller B (2014) Prediction of organic anion-transporting
641 polypeptide 1B1- and 1B3-mediated hepatic uptake of statins based on transporter protein expression and
642 activity data. *Drug Metab Dispos* 42: 1514-1521.
- 643 Lin J, Knight EL, Hogan ML and Singh AK (2003). A comparison of prediction equations for estimating
644 glomerular filtration rate in adults without kidney disease. *J Am Soc Nephrol* 14: 2573-2580.
- 645 Luteijn RD, Zaver SA, Gowen BG, Wyman SK, Garelis NE, Onia L, McWhirter SM, Katibah GE, Corn
646 JE, Woodward JJ and Raulet DH (2019). SLC19A1 transports immunoreactive cyclic dinucleotides.
647 *Nature* 573: 434-438.

- 648 Marloyle M, Lawler SE, Berger G (2019) Current patent and clinical status of stimulator of interferon
649 genes (STING) agonists for cancer immunotherapy. *Pharm. Pat. Anal* 8: 87-90
- 650 Nakai D, Nakagomi R, Furuta Y, Tokui T, Abe T, Ikeda T and Nishimura K (2001) Human liver-specific
651 organic anion transporter, LST-1, mediates uptake of pravastatin by human hepatocytes. *J Pharmacol Exp*
652 *Ther* 297: 861-867.
- 653 Niemi M, Pasanen MK and Neuvonen PJ (2011) Organic anion transporting polypeptide 1B1: a
654 genetically polymorphic transporter of major importance for hepatic drug uptake. *Pharmacol Rev* 63:
655 157-181.
- 656 Nies AT and Keppler D (2007) The apical conjugate efflux pump ABCC2 (MRP2). *Pflugers Arch: Euro*
657 *J Physio* 453: 643-659.
- 658 Pressler H, Sissung TM, Venzon D, Price DK and Figg WD (2011) Expression of OATP family members
659 in hormone-related cancers: potential markers of progression. *PLoS One* 6: e20372.
- 660 Rodgers T, Leahy D, and Rowland M (2005) Physiologically based pharmacokinetic modeling 1:
661 predicting the tissue distribution of moderate-to-strong bases. *J Pharm Sci* 94:1259-1276.
- 662 Rodgers T and Rowland M (2006) Physiologically based pharmacokinetic modelling 2:
663 predicting the tissue distribution of acids, very weak bases, neutrals and zwitterions. *J Pharm Sci*
664 95:1238-1257.
- 665 Rodgers T and Rowland M (2007) Mechanistic approaches to volume of distribution predictions:
666 understanding the processes. *Pharm Res* 24:918-933.
- 667 Swift B, Pfeifer ND and Brouwer KL (2010) Sandwich-cultured hepatocytes: an in vitro model to
668 evaluate hepatobiliary transporter-based drug interactions and hepatotoxicity. *Drug Metab Rev* 42: 446-
669 471.
- 670 Takashima T, Kitamura S, Wada Y, Tanaka M, Shigihara Y, Ishii H, Ijuin R, Shiomi S, Nakae T,
671 Watanabe Y, Cui Y, Doi H, Suzuki M, Maeda K, Kusuhara H, Sugiyama Y and Watanabe Y (2012) PET

672 imaging-based evaluation of hepatobiliary transport in humans with (15R)-11C-TIC-Me. *J Nucl Med* 53:
673 741-748.

674 Tang YQ and Weng N (2013) Salting-out assisted liquid-liquid extraction for bioanalysis. *Bioanalysis* 5:
675 1583-1598.

676 Varma MV, Lai Y, Kimoto E, Goosen TC, El-Kattan AF and Kumar V (2013) Mechanistic modeling to
677 predict the transporter- and enzyme-mediated drug-drug interactions of repaglinide. *Pharm Res* 30: 1188-
678 1199.

679 Varma MV, Steyn SJ, Allerton C and El-Kattan AF (2015) Predicting Clearance Mechanism in Drug
680 Discovery: Extended Clearance Classification System (ECCS). *Pharm Res* 32: 3785-3802.

681 Wang Q, Zheng M and Leil T (2017) Investigating Transporter-Mediated Drug-Drug Interactions Using a
682 Physiologically Based Pharmacokinetic Model of Rosuvastatin. *CPT Pharmacometrics Syst Pharmacol* 6:
683 228-238.

684 Watanabe T, Kusuhara H, Maeda K, Shitara Y and Sugiyama Y (2009) Physiologically based
685 pharmacokinetic modeling to predict transporter-mediated clearance and distribution of pravastatin in
686 humans. *J Pharmacol Exp Ther* 328: 652-662.

687 Wlcek K, Svoboda M, Thalhammer T, Sellner F, Krupitza G and Jaeger W (2008) Altered expression of
688 organic anion transporter polypeptide (OATP) genes in human breast carcinoma. *Cancer Biol Ther* 7:
689 1450-1455.

690 Woo SR, Fuertes MB, Corrales L, Spranger S, Furdyna MJ, Leung MY, Duggan R, Wang Y, Barber GN,
691 Fitzgerald KA, Alegre ML, Gajewski TF (2014) STING-dependent cytosolic DNA sensing mediates
692 innate immune recognition of immunogenic tumors. *Immunity* 41: 830-842.

693 Yang F, Liu L, Chen L, Liu M, Liu F, Xiong Y, Hu X and Xia C (2018) OATP1B3 (699G>A) and
694 CYP2C9*2, *3 significantly influenced the transport and metabolism of glibenclamide and glipizide.
695 *Scientific Reports* 8:18063.

696 Yoshikado T, Toshimoto K, Maeda K, Kusuhara H, Kimoto E, Rodrigues AD, Chiba K and Sugiyama Y
697 (2018) PBPK Modeling of Coproporphyrin I as an Endogenous Biomarker for Drug Interactions

698 Involving Inhibition of Hepatic OATP1B1 and OATP1B3. *CPT: Pharmacometrics Syst Pharmacol* 7:
699 739-747.
700

701 **Figure Legends**

702

703 **Figure 1:** Structure of E7766, a novel agonist of STING pathway

704 **Figure 2:** Phenotyping of hepatobiliary transporters involved in the disposition of E7766. (2A)

705 Uptake of E7766 was evaluated in SLC transporter-expressing HEK293 cells; (2B) Transport of

706 E7766 was evaluated on ABC transporter-expressing membrane vesicles.

707 **Figure 3:** In vitro transporter kinetics of E7766 were measured in HEK-293 cells expression

708 OATP1B1 or OATP1B3. (3A) Kinetics and Michaelis-menten parameters of OATP1B1-

709 mediated uptake of E7766; (3B) Kinetics and Michaelis-menten parameters of OATP1B3-

710 mediated uptake of E7766.

711 **Figure 4:** Pharmacokinetics and disposition of E7766 following intravenous administration in

712 wild type and OATP1B1/1B3 humanized mice. (4A) Plasma concentrations of E7766 were

713 measured with or without coadministration with Rifampicin following intravenous

714 administration of E7766 and Rifampicin. (4B) Blood concentrations of E7766 were measured

715 with or without coadministration with Rifampicin following intravenous administration of E7766

716 and Rifampicin. (4C) Excretion with or without coadministration with Rifampicin of E7766 in

717 urine, bile and feces was determined following intravenous administration of E7766 and

718 Rifampicin. (WT: wild type mouse; Hu: Humanized mouse)

719 **Figure 5** Summary of PK parameters and DDI profile of E7766 from PBPK model. (5A)

720 Contribution of passive diffusion, OATP1B1 and OATP1B3-mediated uptake to overall hepatic

721 uptake clearance of E7766. Simulated plasma (5B) and liver (5C) concentration-time profiles of

722 E7766 following i.v. administration of 1 mg dose with and without 600 mg oral dose of

723 Rifampicin. Sensitivity analysis of changes in E7766 area under the curve ratio (AUCR) as a
724 function of REF (5D) and kinetic parameters for OATP1B1 (5E) and OATP1B3 (5F).
725

726 **Tables**

727 **Table 1**

728 Summary of in vitro parameters for E7766 estimated from the sandwich cultured human hepatocytes

Test Article	Target Concentration (μmol/L)	Temperature	Time (min)	Uptake $CL_{int,T}$ (μL/min/10 ⁶ cells)	Efflux $CL_{int,T}$ (μL/min/10 ⁶ cells)	BEI %
E7766	0.3	37°C	1	7.69 ± 0.47	—	—
			5	3.83 ± 0.26	—	—
			10	3.12 ± 0.26	—	—
			20	Not determined	2.05 ± 0.07	85.2 ± 1.7
		4°C	10	0.13 ± 0.00	—	—
	1.0	37°C	1	5.46 ± 0.10	—	—
			5	2.70 ± 0.14	—	—
			10	1.85 ± 0.13	—	—
			20	Not determined	1.42 ± 0.08	86.2 ± 0.40
		4°C	10	0.14 ± 0.02	—	—
	10.0	37°C	1	1.22 ± 0.11	—	—
			5	0.47 ± 0.02	—	—
			10	0.33 ± 0.01	—	—
			20	Not determined	0.15 ± 0.01	70.9 ± 1.3
		4°C	10	0.58 ± 0.73	—	—
	d8-TCA	5	37°C	10	14.2 ± 0.82	11.0 ± 1.74
4°C			0.27 ± 0.02		—	—
Rosuvastatin	10	37°C	10	6.22 ± 0.31	2.23 ± 0.38	42.7 ± 5.8
		4°C		0.21 ± 0.04	—	—

729 Uptake $CL_{int,T}$, intrinsic hepatic uptake clearance; Efflux $CL_{int,T}$, intrinsic biliary efflux clearance; BEI, biliary excretion
 730 index; d8-TCA, deuterium-labeled sodium taurocholate. Values represent the means ± SD (n = 3)

731

732

733 **Table 2**

734 Disposition of E7766 in bile duct cannulated (BDC) rat and dog following intravenous bolus administration

Dose	BDC Rat IV bolus, 1 mg/kg	Dog IV bolus, 0.075 mg/kg
CL _{tot,p} (L/h/kg)	6.50 ± 0.429	1.29 ± 0.369
V _{ss} (L/kg)	2.47 ± 0.849	0.553 ± 0.345
A _{e renal} (%)	13.7 ± 2.80	4.96 ± 4.37
CL _{renal} (L/h/kg)	0.895 ± 0.189	0.0528 ± 0.0293
A _{e biliary} (%)	92.1 ± 7.26	87.9 ± 30.5
CL _{biliary} (L/h/kg)	6.04 ± 0.798	1.19 ± 0.637
A _{e fecal} (%)	0.366 ± 0.208	—
CL _{fecal} (L/h/kg)	0.0227 ± 0.0138	—

735 CL_{tot,p}, total plasma clearance; V_{ss}, distribution volume at steady state; A_{e renal}, amount excreted in urine; CL_{renal}, renal
 736 excretory clearance; A_{e biliary}, amount excreted in bile; CL_{biliary}, hepatobiliary excretory clearance; A_{e fecal}, amount excreted
 737 in feces; CL_{fecal}, fecal excretory clearance. Values represent the means ± SD (n = 4 for BDC rats and n = 3 for dogs)

738

739 **Table 3**

740 Liver and systemic exposure of E7766 in wild type and humanized mice in the presence or the absence of Rifampicin.

Parameters	WT Mice 0.5 mg/kg E7766	WT Mice 0.5 mg/kg E7766 +Rifampicin	Hu Mice 1.0 mg/kg E7766	Hu Mice 0.5 mg/kg E7766 +Rifampicin
AUC _{total} (ng·h/mL)	56.0	300	126 ± 48.7	302 ± 92.2
AUC _{total} /Dose (ng·h/mL/[mg/kg])	112	600	126 ± 48.7	604 ± 184
CL _{tot,p} (L/h/kg)	8.93	1.72	9.20 ± 4.65	1.80 ± 0.619
V _{ss} (L/kg)	1.66	0.520	5.93 ± 5.96	1.29 ± 0.243
Liver AUC _{total} (ng·h/g)	4460	4250	—	—
Liver K _{p,total}	79.6	14.2	—	—

741 WT, Wild type mouse; Hu, OATP1B1/OATP1B3 humanized mouse; AUC_{total}, area under the total plasma concentration-
 742 time curve; AUC_{total}/Dose, area under the total plasma concentration-time curve normalized by dose; CL_{tot,p}, total plasma
 743 clearance; V_{ss}, distribution volume at steady state; Liver AUC_{total}, area under the total liver concentration-time curve; Liver
 744 K_{p,total}, total liver-to-plasma concentration ratio. Values represent the means ± SD (n = 3)

Table 4

Summary of input parameters used to build the PBPK model for E7766.

Downloaded from dnd.aspejournals.org at ASPET Journals on April 18, 2024

Parameter	Scenario one	Scenario two	Source
<i>PhysChem and Blood Binding</i>			
Mol Weight (g/mol)	746	746	Calculated
log P	1.31	1.31	Measured
Compound Type	Monoprotic Acid	Monoprotic Acid	—
pKa	3.41	3.41	Calculated
B/P	0.55	0.55	Measured
f_u	0.50	0.50	Measured
Distribution Model	Full PBPK Model	Full PBPK Model	—
V_{ss} (L/kg)	0.637	0.637	SimCYP predicted (Method 2, the Rodgers-Rowland method)
K_p scalar	4.0	4.0	fitted based on preclinical data, see Methods for details
CL_{renal} (L/h)	3.0	3.0	Estimate as $f_u \times GFR$
<i>Hepatic Transport (permeability-limited liver module)</i>			
Passive diffusion CL_{PD} (mL/min/ 10^6 cells)	0.00013	0.00013	Obtained from E7766 uptake measured at 0.3 μ mol/L at 4 °C with SCHH model (Table 1)
f_{uIW}	1.00	1.00	SimCYP predicted
f_{uEW}	0.657	0.657	SimCYP predicted

J_{\max} (pmol/min/10 ⁶ cells) for OATP1B1	8.34	—	V_{\max} in the unit of pmol/min/mg protein (Figure 3) was converted to J_{\max} in the unit pmol/min/10 ⁶ cells by incorporating measured protein abundance data of HEK293 cells (0.3 mg protein per 10 ⁶ HEK293 cells)
K_m (μmol/L) for OATP1B1	2.20	—	Obtained from transporter kinetic assays (Figure 3)
f_{uinc} for OATP1B1	1.00	—	SimCYP predicted
REF for OATP1B1	0.10	—	Calculated by Equation 4, see Supplemental Table 2 for details of transporter protein expression.
J_{\max} (pmol/min/10 ⁶ cells) for OATP1B3	24.39	—	Figure 3. Units were converted as shown above for OATP1B1
K_m (μmol/L) for OATP1B3	3.97	—	Obtained from transporter kinetic assays (Figure 3)
f_{uinc} for OATP1B3	1.00	1.00	SimCYP predicted
REF for OATP1B3	2.80	—	Calculated by Equation 5, see Supplemental Table 2 for details of transporter protein expression.
Uptake $CL_{\text{int,T}}$ (μL/min/10 ⁶ cells)	—	7.7	For scenario two, the uptake $CL_{\text{int,T}}$ for E7766 measured at 0.3 μmol/L after 1 min incubation at 37 °C (Table 1) was assigned as input value for uptake $CL_{\text{int,T}}$ in SCHH, as early time point and lower concentration can better represent the initial linear uptake phase.
REF _{SCHH}	—	1	The REF _{SCHH} is assumed to be one based on literature reported data shown that OATP1B1 and OATP1B3 expression levels are comparable between SCHH and primary hepatocyte if from the same lot (Kimoto et al., 2012)
Efflux $CL_{\text{int,T}}$ (μL/min/10 ⁶ cells)	2.1	2.1	For both scenarios one and two, SCHH efflux $CL_{\text{int,T}}$ for E7766 measured at 0.3 μmol/L after 20 min incubation at 37 °C (Table 1) was used as input value for Efflux $CL_{\text{int,T}}$.

B/P, blood-to-plasma partition ratio; f_i , unbound drug fraction in plasma; V_{ss} , distribution volume at steady state; K_p , tissue-to-plasma partition coefficients; CL_{renal} , renal excretory clearance; CL_{PD} , passive diffusion clearance; f_{iW} , unbound drug fraction in intracellular water; f_{eW} , unbound drug fraction in extracellular water; f_{uinc} , unbound drug fraction in in-vitro incubation system; K_m , Michaelis-Menten constant; J_{\max} , in vitro maximum rate of transporter mediated uptake or efflux; REF, relative

expression factor; Uptake $CL_{int,T}$, intrinsic uptake clearance obtained from SCHH assay; Efflux $CL_{int,T}$, intrinsic biliary efflux clearance obtained from SCHH assay. For scenario one, hepatic uptake clearance was assigned from the transporter kinetics measured in HEK 293 cells and for scenario two, intrinsic active uptake clearance measured in from SCHH was assigned to OATP1B3.

Table 5

Summary and comparison of simulated PK and DDI parameters of E7766 from PBPK models using two scenarios. Simcyp default compound for rifampicin was used for simulations. For scenario one, hepatic uptake clearance was assigned from the transporter kinetics measured in HEK 293 cells and for scenario two, intrinsic active uptake clearance measured in from SCHH was assigned to OATP1B3.

PKPD profile parameters of E7766	Scenario one		Scenario two	
	(-) Rifampicin	(+) Rifampicin	(-) Rifampicin	(+) Rifampicin
AUC _{total} (nmol·h/L)	47.38	131.06	67.26	174.07
AUC _{total} ratio	2.77		2.59	
C _{max,tot} (nmol/L)	474.01	479.92	476.24	480.12
C _{max,tot} ratio	1.01		1.01	
CL _{tot,p} (L/h)	29.62	11.88	21.55	8.66
CL _{tot,p} ratio	0.40		0.40	
Liver intracellular AUC _{free} (nmol·h/L)	76.19	69.06	71.35	61.28
Liver intracellular AUC _{free} ratio	0.91		0.86	

AUC_{total}, area under total plasma concentration-time curve; AUC_{total} ratio, ratio of AUC_{total} in the presence and absence of the inhibitor; C_{max,tot} maximum total plasma concentration; C_{max,tot} ratio, ratio of C_{max,tot} in the presence and absence of the inhibitor; CL_{tot,p}, total plasma clearance; CL_{tot,p} ratio, ratio of CL_{tot,p} in the presence and absence of the inhibitor; Liver intracellular AUC_{free}, area under free intra-hepatocellular concentration-time curve; Liver intracellular AUC_{free} ratio, ratio of area under free intra-hepatocellular concentration-time curve in the presence and absence of the inhibitor.

Figures

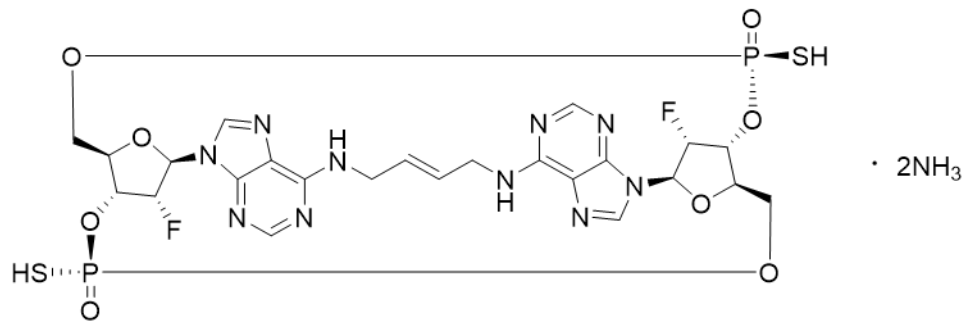
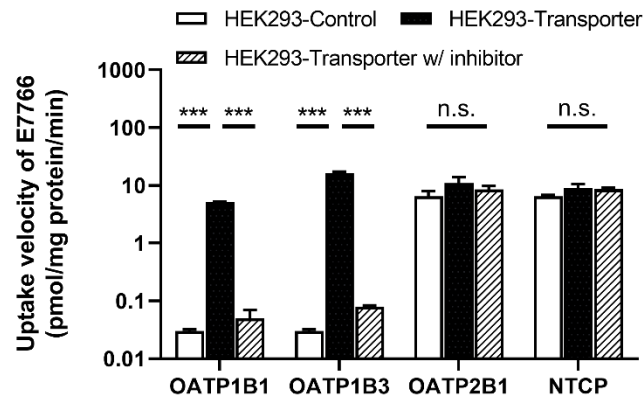


Figure 1

2A



2B

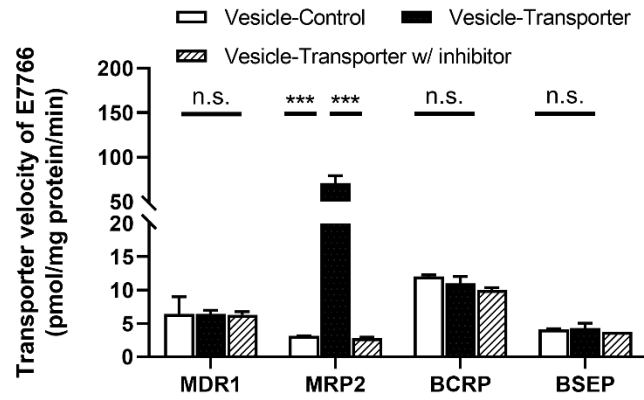


Figure 2

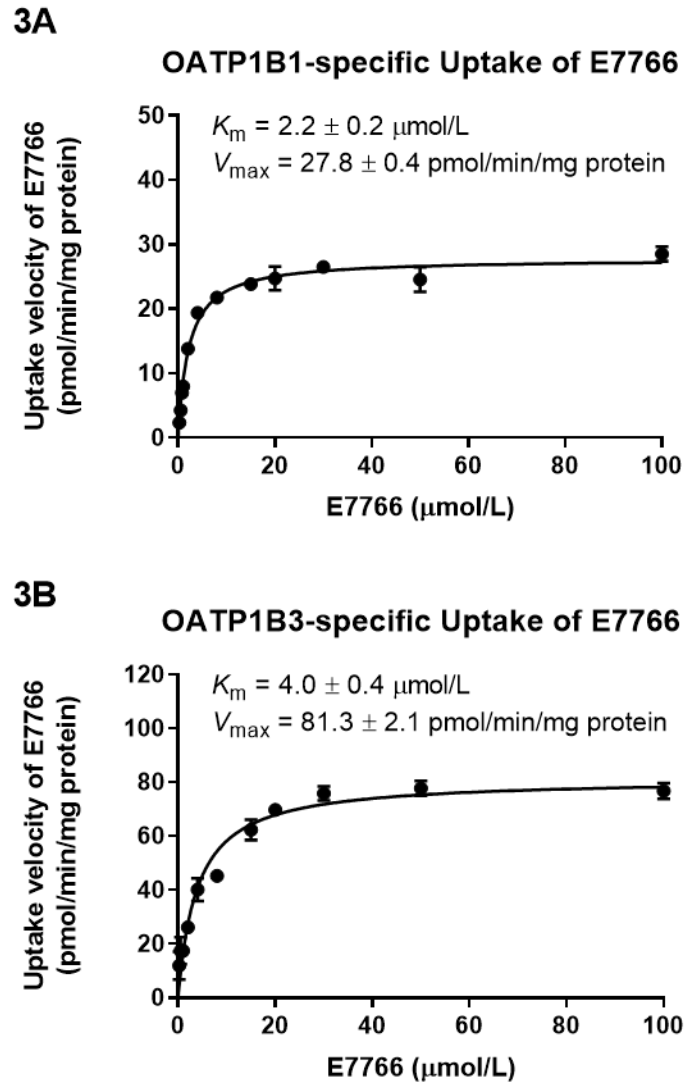


Figure 3

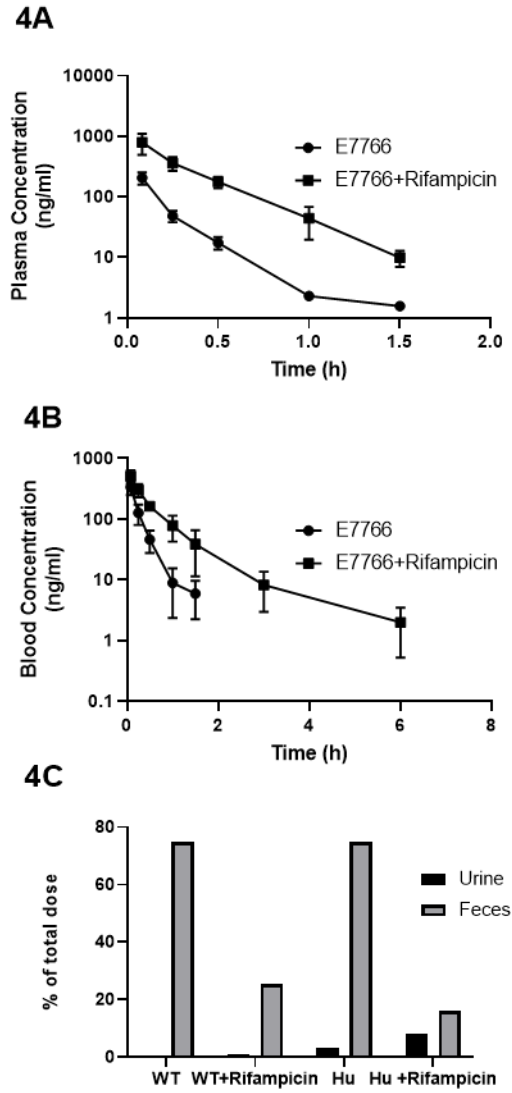


Figure 4

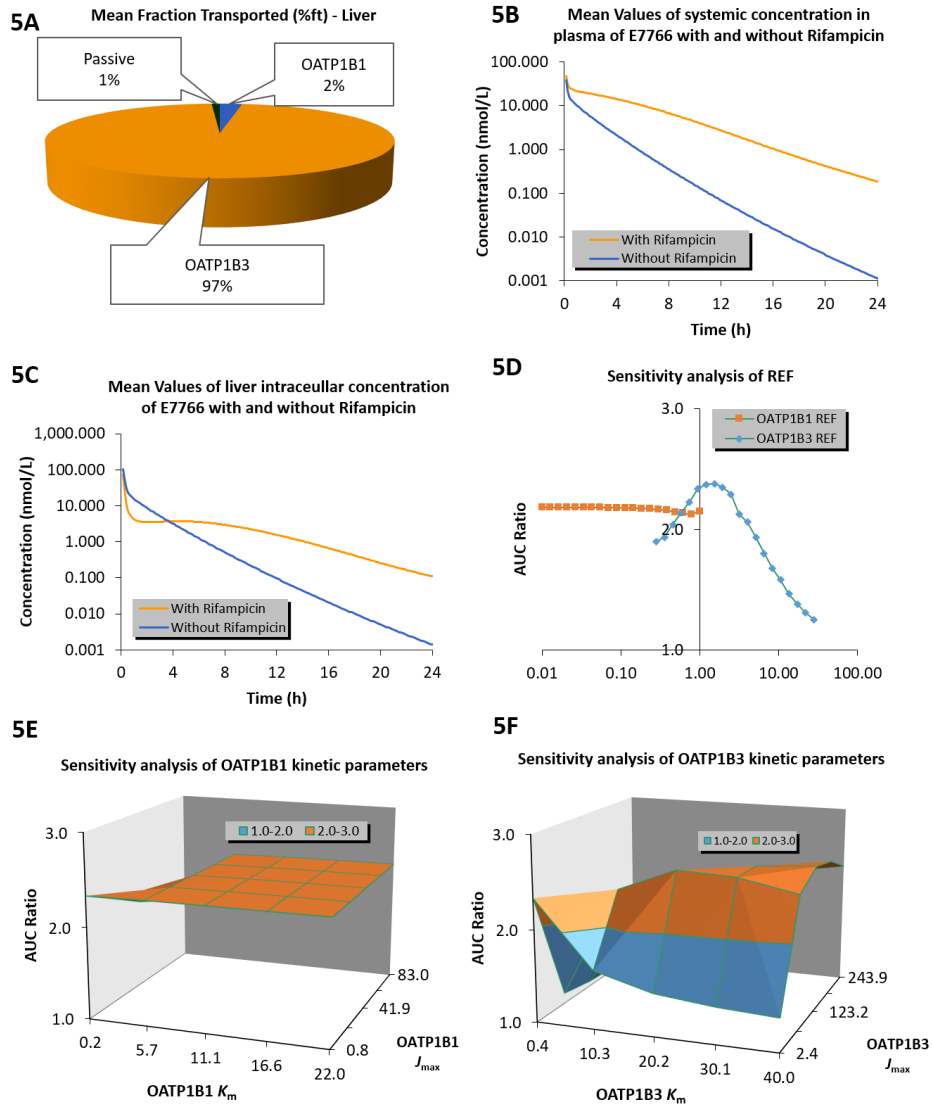
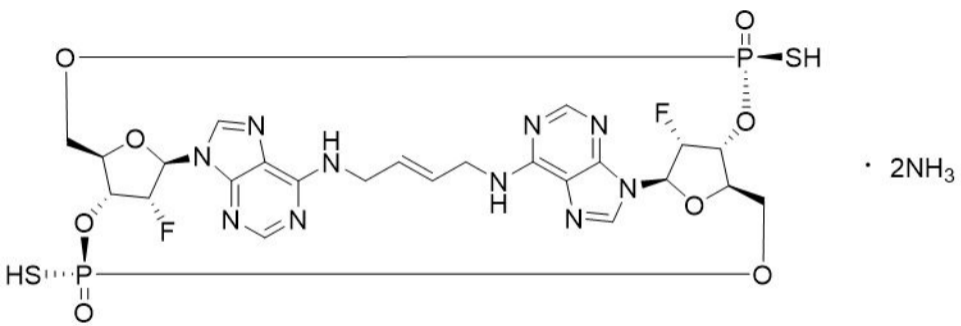
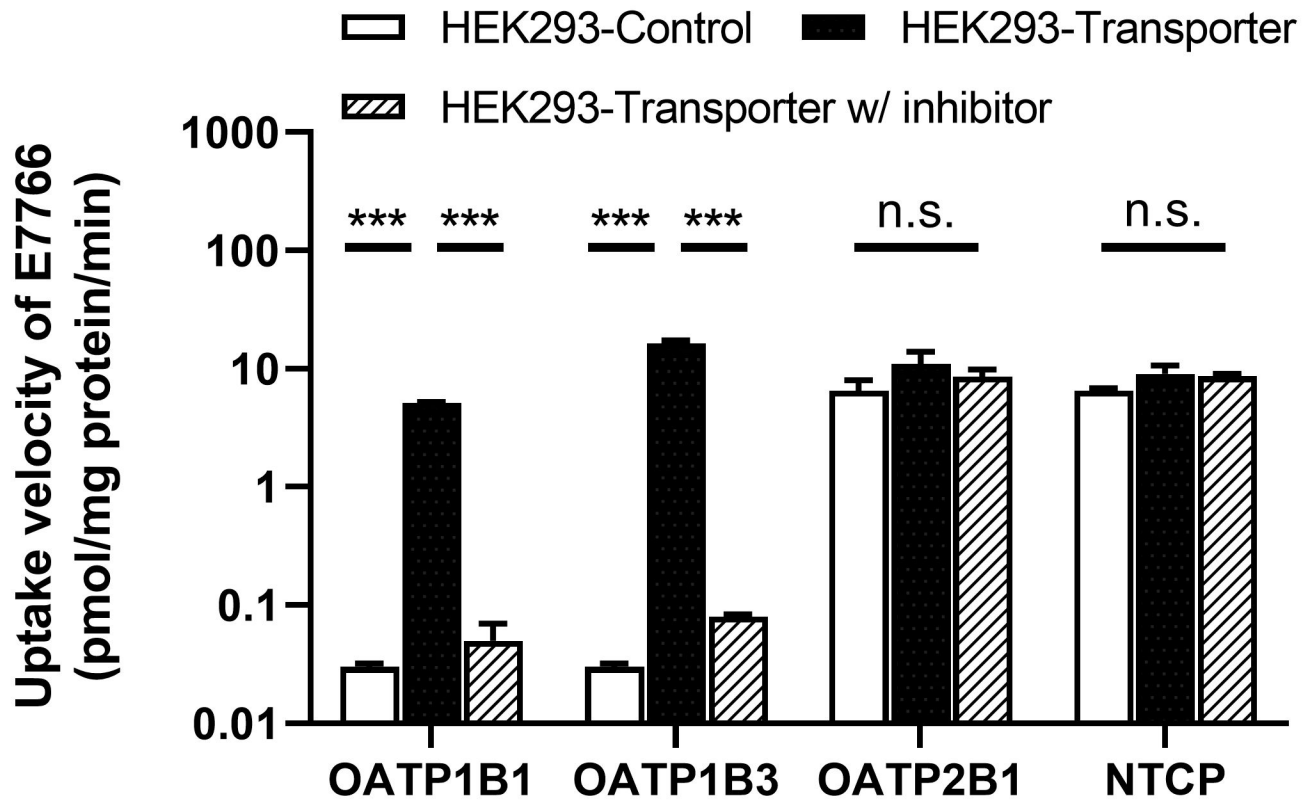


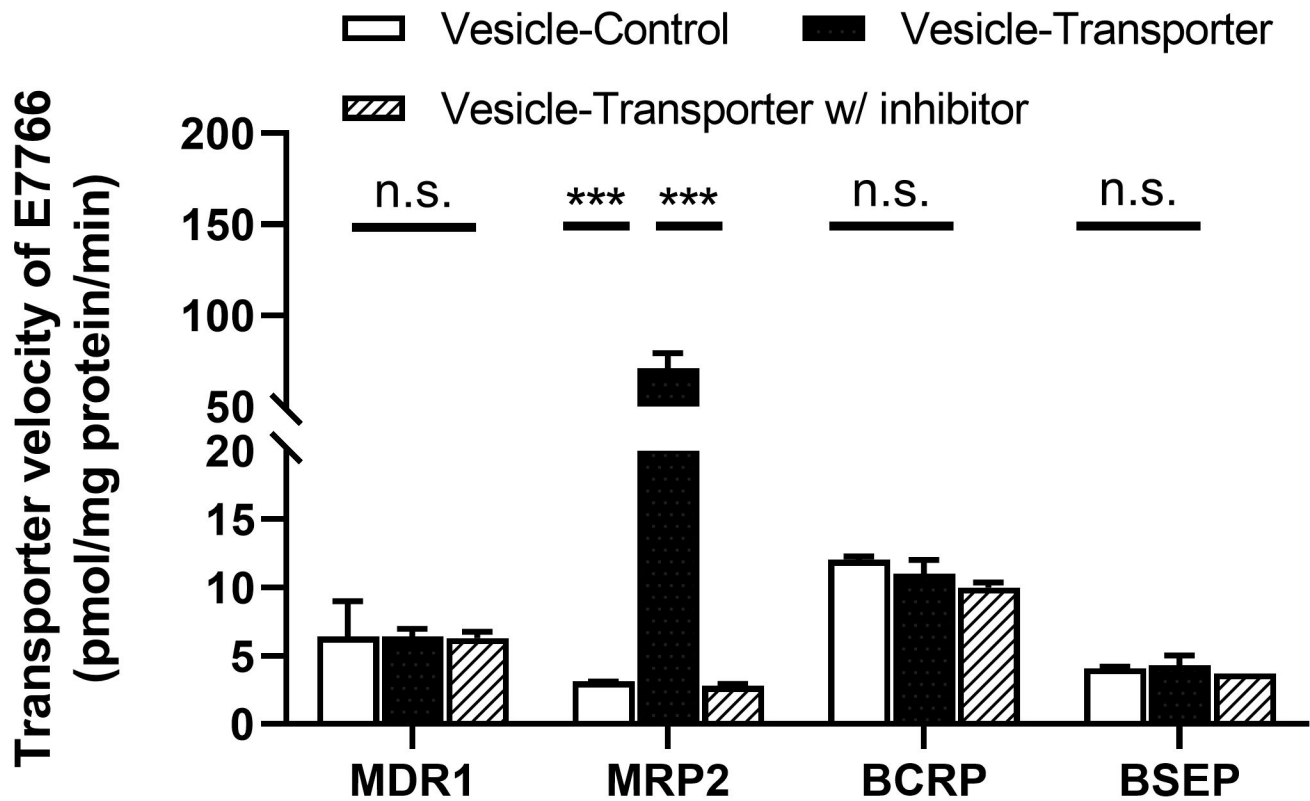
Figure 5

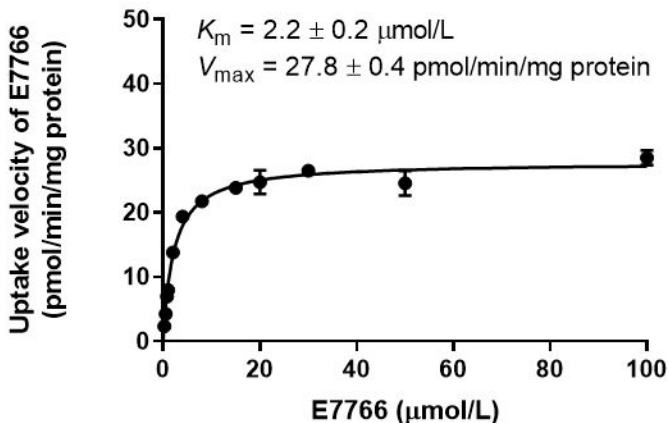
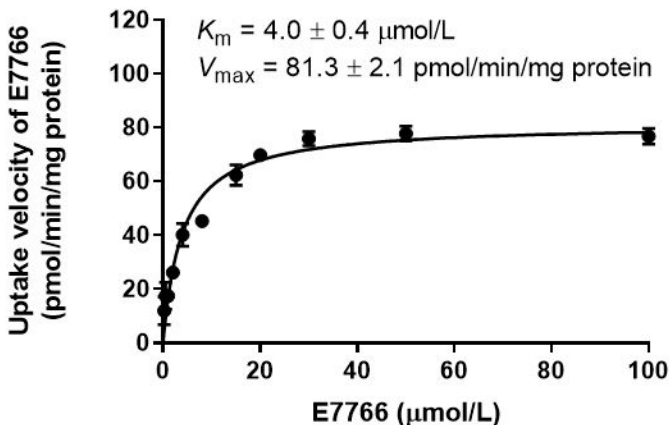


2A

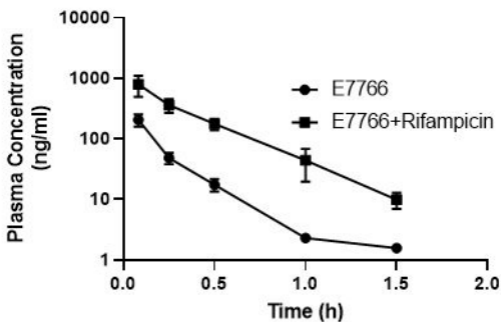


2B

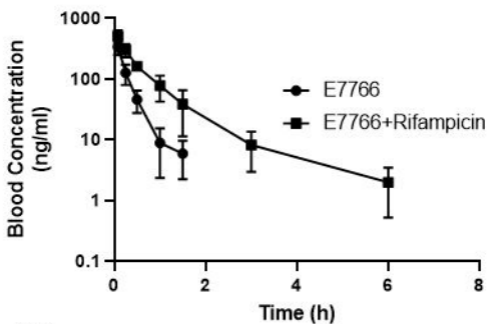


3A**OATP1B1-specific Uptake of E7766****3B****OATP1B3-specific Uptake of E7766**

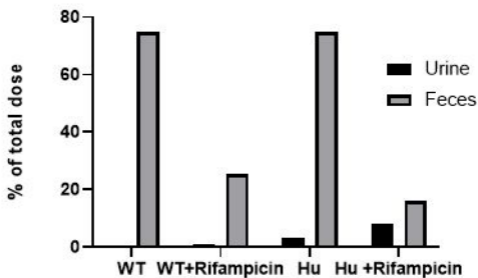
4A



4B

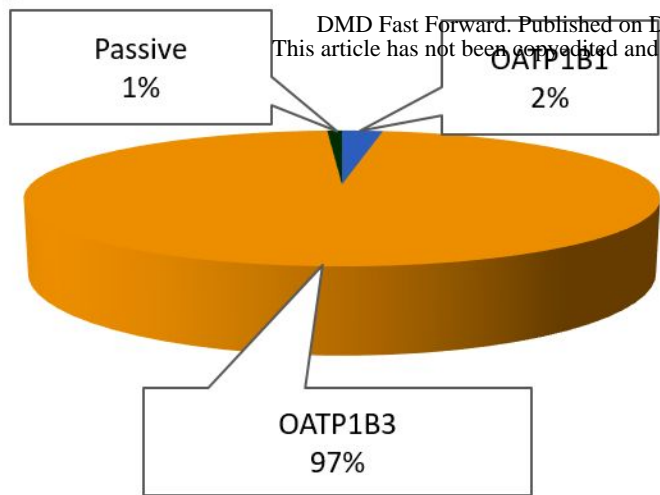


4C



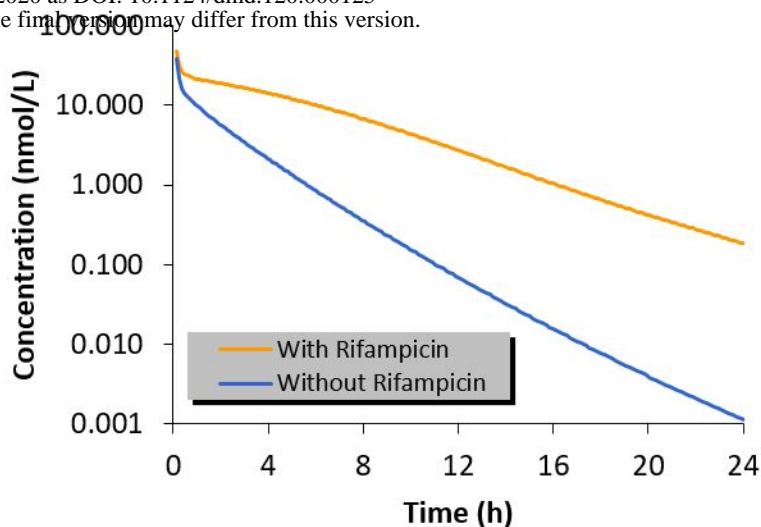
5A

Mean Fraction Transported (%ft) - Liver



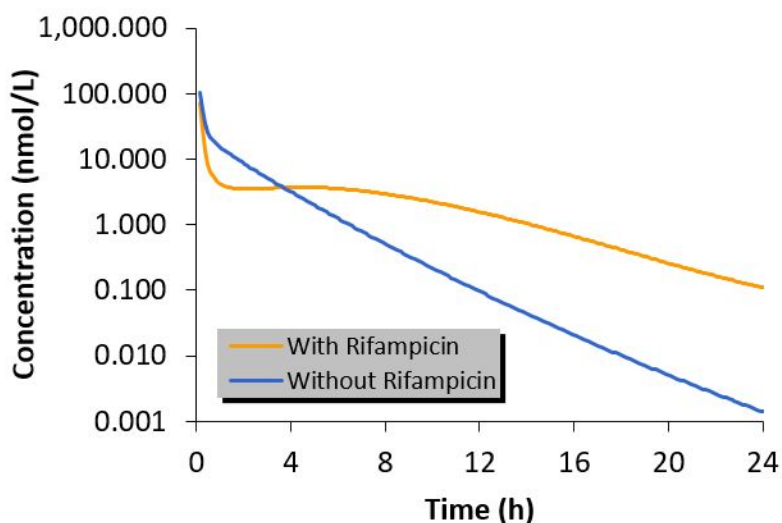
5B

Mean Values of systemic concentration in plasma of E7766 with and without Rifampicin



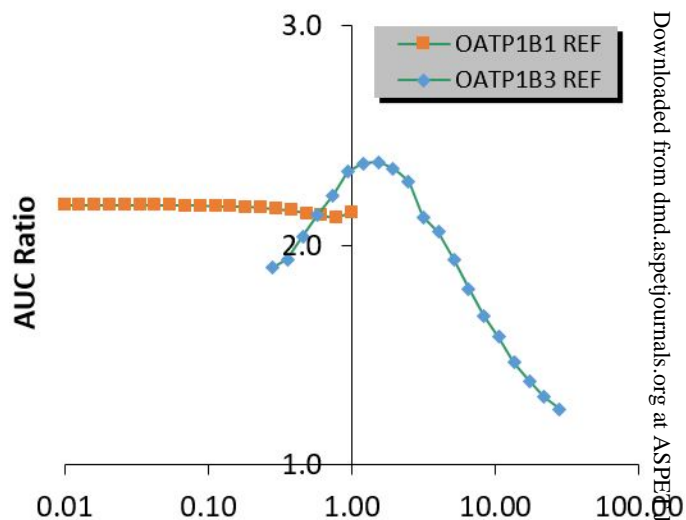
5C

Mean Values of liver intracellular concentration of E7766 with and without Rifampicin



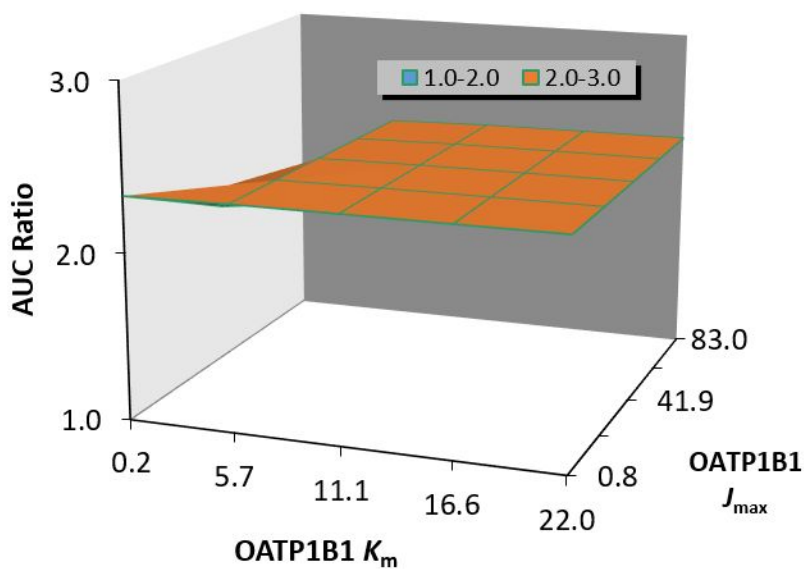
5D

Sensitivity analysis of REF



5E

Sensitivity analysis of OATP1B1 kinetic parameters



5F

Sensitivity analysis of OATP1B3 kinetic parameters

